International Journal of Nanomedicine

Dovepress
open access to scientific and medical research

Open Access Full Text Article

ORIGINAL RESEARCH

Nasal Administration of bFGF-Loaded Nanoliposomes Attenuates Neuronal Injury and Cognitive Deficits in Mice with Vascular Dementia Induced by Repeated Cerebral Ischemia–Reperfusion

Ming Zhang[1], Shuai-shuai Huang[1], Wen-yue He[1], Wei-juan Cao[2], Min-yi Sun[1], Ning-wei Zhu[2]

[1]Department of Pharmacy, Ningbo Yinzhou NO.2 Hospital, Ningbo, Zhejiang, 315100, People's Republic of China; [2]Department of Pharmacy, Zhejiang Pharmaceutical University, Ningbo, Zhejiang Province, 315100, People's Republic of China

Correspondence: Ning-wei Zhu, Email NingweiZhu@126.com

Introduction: Basic fibroblast growth factor (bFGF) shows great potential for preventing vascular dementia (VD). However, the blood–brain barrier (BBB) and low bioavailability of bFGF in vivo limit its application. The present study investigated how nasal administration of bFGF-loaded nanoliposomes (bFGF-lips) affects the impaired learning and cognitive function of VD mice and the underlying mechanism involved.

Methods: A mouse model of VD was established through repeated cerebral ischemia–reperfusion. A Morris water maze (MWM) and novel object recognition (NOR) tests were performed to assess the learning and cognitive function of the mice. Hematoxylin and eosin (HE) staining, Nissl staining and TUNEL staining were used to evaluate histopathological changes in mice in each group. ELISA and Western blot analysis were used to investigate the molecular mechanism by which bFGF-lips improve VD incidence.

Results: Behavioral and histopathological analyses showed that cognitive function was significantly improved in the bFGF-lips group compared to the VD and bFGF groups; in addition, abnormalities and the apoptosis indices of hippocampal neurons were significantly decreased. ELISA and Western blot analysis revealed that bFGF-lips nasal administration significantly increased the concentrations of superoxide dismutase (SOD), glutathione peroxidase (GSH-Px), bFGF, B-cell lymphoma 2 (Bcl-2), phosphorylated protein kinase B (PAKT), nuclear factor erythroid 2-related factor 2 (Nrf2), NAD(P)H quinone oxidoreductase 1 (NQO1) and haem oxygenase-1 (HO-1) in the hippocampus of bFGF-lips mice compared with the VD and bFGF groups. Furthermore, the concentrations of malondialdehyde (MDA), caspase-3 and B-cell lymphoma 2-associated X (Bax) were clearly lower in the bFGF-lips group than in the VD and bFGF groups.

Conclusion: This study confirmed that the nasal administration of bFGF-lips significantly increased bFGF concentrations in the hippocampi of VD mice. bFGF-lips treatment reduced repeated I/R-induced neuronal apoptosis by regulating apoptosis-related protein concentrations and activating the phosphatidylinositol-3-kinase (PI3K)/(AKT)/Nrf2 signaling pathway to inhibit oxidative stress.

Keywords: bFGF, nanoliposomes, vascular dementia, nasal administration, oxidative stress, neuronal apoptosis

Introduction

Vascular dementia (VD) is a progressive disease that affects individuals' cognitive ability and is caused by various acute or chronic cerebrovascular diseases. VD is the second leading cause of dementia,[1,2] with Alzheimer's disease (AD) being the leading cause.[3] Most VD patients suffer from slowed thinking, impaired memory, depression, and a loss of executive functions, which seriously affect their daily lives.[4] Specific strategies for the treatment or prevention of VD are greatly needed but currently limited.[5,6]

Cerebral ischemia is closely associated with the development and progression of VD and AD.[7] An obvious reduction in regional cerebral blood flow causes glucose and oxygen deprivation. These events then lead to the activation of oxidation.[8] The overproduction of reactive oxygen species (ROS) resulting from ischemic injury is a major mechanism that underlies VD.[9,10] A decrease in endogenous antioxidants has been reported to cause an increase in oxidative stress.[11]

Received: 27 November 2023
Accepted: 7 February 2024
Published: 12 February 2024

ROS can react with substrates important for the survival of neurons, including proteins, lipids, and DNA, resulting in neuropathological lesions and brain damage.[12] Hence, drugs that can regulate oxidative stress may show therapeutic potential for treating VD.

The neurotrophic factors and cytokines that are produced in response to brain injury and oxidative stress may protect neurons against injuries relevant to the pathogenesis of VD. For example, basic fibroblast growth factor (bFGF) is a modulatory ligand for neurogenesis, is expressed in neurogenic niches and plays an important role in the proliferation and differentiation of adult neural stem and progenitor cells; as a result, bFGF has been implicated in the control of adult neurogenesis.[13,14] An animal study confirmed that exogenous bFGF infusions reversed depressive-like behaviors and impaired hippocampal neurogenesis by inhibiting neuroinflammation.[15] Moreover, studies of cultured neurons have provided evidence that bFGF can suppress the oxidative stress and mitochondrial dysfunction induced by amyloid β-peptide and Fe in synaptosomes.[16] However, as bFGF has a molecular weight of 16.5 kDa, the protein cannot easily cross the blood–brain barrier (BBB).[17] Therefore, investigations into alternative methods of delivering bFGF to the brain have been performed.

Intranasal administration is an alternative method that has been investigated, and it is particularly attractive because substances are delivered directly to the central nervous system (CNS); the system utilizes pathways through the olfactory and trigeminal nerves that innervate the nasal passages and eliminates the need for and potential risks of peripheral intravenous or intracerebroventricular administration.[18] However, despite the potential of nasal drug delivery, several factors limit the intranasal absorption of drugs. The major barriers include physical removal from the site of deposition in the nasal cavity by mucociliary clearance mechanisms, enzymatic degradation in the mucus layer and nasal epithelium and low permeability of the nasal epithelium.[19]

The use of a suitable drug delivery system has attracted great interest for overcoming the aforementioned nasal barriers and improving nasal drug absorption. Novel nanodrug delivery systems, including nanoliposomes, nanoparticles and other polymeric nanosystems, have demonstrated great efficacy in increasing the bioavailability of drugs administered through the nasal route.[19–21] The poor membrane permeability of normal nanoparticles caused by limited endocytosis in the nasal mucosa restricts their application as brain drug delivery carriers.[22] Bioactive peptides, such as cell-penetrating peptides (CPPs), are used to modify the surface of nanoparticles and enhance nasal mucosal transport of nanoparticles to the brain. However, the toxicity of CPP-mediated delivery remains a concern.[23] Moreover, most polymeric nanosystems involve cationic polymers, such as chitosan and PEG. Cationic polymers interact with the negatively charged surface of the mucosal membrane and cause toxicity.[23] As small vesicles enclosed by lipid bilayer membranes, nanoliposomes consist of naturally occurring lipids and may be nontoxic.[24] The nasal clearance half-life of nanoliposomes is four times greater than the normal clearance half-life of the human nose, suggesting the mucoadhesion ability of nanoliposomes and the potential of nasal application.[25] Nanoliposomes are efficient vehicles for delivering therapeutic proteins to the CNS because they exhibit high solubility and bioavailability, exhibit low toxicity and are nonimmunogenic.[26–28] Thus, administering nanoliposomes through nasal delivery shows considerable potential for the delivery of bFGF to the CNS.

Ischemia–reperfusion-induced regional cerebral injury is among the most commonly employed models for establishing VD in animals.[6] In this study, we prepared and characterized nanoliposomes encapsulating bFGF, and we showed that this formulation could deliver the protein efficiently to the mouse brain when administered via the intranasal route. We subsequently evaluated whether bFGF exerted a neuroprotective effect on global cerebral ischemia-induced VD in mice and explored the underlying mechanisms involved.

Materials and Methods

Preparation and Characterization of bFGF-Loaded Nanoliposomes

Based on our previous research,[29] bFGF-loaded nanoliposomes (bFGF-lips) were prepared by the reverse-phase evaporation method. Briefly, to prepare the phospholipid membrane, 90 mg of hydrogenated soy phosphatidylcholine (HSPC) (Shanghai AVT) and 10 mg of cholesterol (Shanghai AVT) were completely dissolved in 1 mL of dichloromethane (Guangdong Guanghua Technology Co., Ltd.) at room temperature. Then, 100 μL of bFGF (mouse-derived, PeproTech) solution (10 mg/mL) was added dropwise to the dichloromethane solution at 4°C, followed by ultrasonication with an ultrasonic probe (50 W, 2 s on, 3 s off, 1 min) until a water-in-oil emulsion was formed. The

dichloromethane was removed by rotary evaporation under reduced pressure (25°C, 0.08MPa). Finally, the residual dry lipid membrane was hydrated with phosphate-buffered saline (PBS) (pH 7.4, 10×10^{-3} mol) and rotated and evaporated (25°C, 0.08 MPa) until a transparent bFGF-lips suspension was formed. The bFGF-lips were then passed through a 0.22 μm microporous filtration membrane three times, and bFGF-lips solution containing 0.75 mg/mL bFGF was obtained. Blank nanoliposomes (blank-lips) were prepared by replacing the bFGF solution with an equal volume of distilled water.

The morphology of the bFGF-lips and blank nanoliposomes was observed via a transmission electron microscope (TEM) (1230, Jeol Jem Company, Tokyo, Japan) operated at 120 kV. For TEM sample preparation, the bFGF-lips and blank nanoliposome solutions prepared above were first diluted 10 times with distilled water. Then, 10 μL of each diluted solution was added dropwise to a carbon-coated grid for 30s, and the excess solution was aspirated using filter paper. The grids were stained with 2% phosphotungstic acid for 1 min and dried overnight at room temperature.

The particle size, size distribution and zeta potential of bFGF-lips and blank nanoliposomes were determined by dynamic light scattering (DLS) analysis using a Malvern Zetasizer Nano ZS90 (Malvern Instruments, Malvern, UK) at a 90°C scattering angle and 25 °C in a cell with a 1 cm width. The bFGF-lips and blank nanoliposome solutions were first diluted 100-fold using distilled water before size determination.

The encapsulating efficiency of bFGF-lips was determined by enzyme-linked immunosorbent assay (ELISA) as previously described.[30] Then, 1.5 mL of the bFGF-lips dispersion was centrifuged at 10,000 × g for 30 minutes. The supernatant was collected and diluted for ELISA. The analyses were performed in triplicate, and the encapsulation efficiency (EE) was calculated as follows:

$$\text{Encapsulation efficiency (\%)} = (\text{total amount of bFGF} - \text{amount of bFGF in the supernatant}) / \text{total amount of bFGF} \times 100\%.$$

To investigate bFGF release, bFGF-lips solution (2 mL) was first placed into a dialysis bag (Spectra/Por CE Biotech Membrane; Spectrum Laboratories, Inc., Rancho Dominguez, CA, USA) (molecular weight cutoff = 20 kDa). Release was then performed in 100 mL of PBS (pH 7.4) at 37°C in a shaking water bath at 150 rpm. The release medium (5 mL) was withdrawn and replaced with an equivalent volume of fresh medium at different time points (0, 1, 3, 6, 9, 12, 18, 24, 30, 36, 42 54, 66 and 78 hours). The concentration of bFGF in the release medium was assayed by using an ELISA kit. The following formula was used to calculate the cumulative release percentage: cumulative release percentage(%)=(amount of bFGF released/total bFGF in liposomes)×100%.

According to previous methods,[31] the stability of bFGF-lips was evaluated by measuring the EE, bioactivity and physical stability (K_E) of bFGF-lips at different temperatures (4, 25, 30 and 40°C) under exposure to 4100 lx light at room temperature (20±2°C). For K_E detection, 1 mL of bFGF-lips was centrifuged at 3500 rpm for 10 min, after which the supernatant was collected. A volume of 0.3 mL of bFGF-lips solution before centrifugation and 0.3 mL of bFGF-lips in supernatant solution after centrifugation were taken and diluted to 5 mL with PBS (pH 6.8) solution. The absorbances (pre- and postcentrifugation absorbances: A_0 and A_1, respectively) were measured at 500 nm. The value of K_E was calculated with the following equation: $K_E=(A_0 - A_1)/A_0 \times 100\%$. The bioactivity of bFGF-lips was determined by the MTT method as described in our previous study.[32] Moreover, the EE was determined as described above. All the experiments for liposome characterization were repeated three times.

Experimental Animals

A total of fifty female ICR mice weighing 30–35 g were obtained from the Laboratory Animal Centre of Zhejiang Experimental Animal Centre and were housed in a light-controlled room (14-h light/10-h dark cycle) at a consistent temperature (24±2°C). The animal care and experimental procedures were in accordance with the principles of the Animal Ethics Committee of Zhejiang Pharmaceutical College, which approved this study (202105023). Animal health and behavior were monitored daily.

Establishment of the VD Mouse Model

The ischemia–reperfusion-induced VD mouse model was established under aseptic conditions through bilateral common carotid artery occlusion (BCCAO) according to a previously published method with some modifications.[33] The mice

were anesthetized using thiopental sodium (45 mg/kg i.p.). The bilateral common carotid arteries were exposed and gently separated from the carotid sheath and vagus nerve via a midline cervical incision. The bilateral common carotid arteries were ligated with 4–0 silk sutures for 20 min. Thereafter, the sutures were removed, and blood flow was restored. After the blood flow had been restored for 10 min, the bilateral common carotid was further ligated for 20 min. This process was repeated three times. After the third reperfusion, the mice were observed carefully for 40 min, and the cervical incision was closed with sutures. Then, the mice were placed under a heat lamp to prevent hypothermia until they completely recovered from general anesthesia. The sham group mice underwent the same procedure but without carotid artery ligation.

Experimental Design and Grouping

The fifty mice were randomly divided into the following groups (n=10 per group). (1) Sham group: control mice, which underwent the surgical procedure but without carotid artery ligation and were nasally administered 2 μL of PBS; (2) VD group: VD mice were nasally administered 2 μL of PBS; (3) blank nanoliposomes (blank-lips) group: VD mice were nasally administered blank lips in 2 μL of PBS; (4): bFGF group: VD mice were nasally administered free bFGF solution (15 μg/kg) in 2 μL of PBS; and (5): bFGF-loaded nanoliposomes (bFGF-lips) group: VD mice were nasally administered bFGF-lips solution (15 μg/kg) in 2 μL of PBS. The nasal administration method was described in our previous study but was performed in this study with some modifications.[17] Briefly, the mice remained supine with their head in a horizontal position. The nasal administration was performed using gentle pipetting of 1 μL of solution per nostril, which was naturally sniffed in by the mouse, with a 3-min interval between nostril administrations. All the treatments were administered once a day for 28 consecutive days starting at 1 h after surgery.

In accordance with previous methods used to determine the cerebral distribution of bFGF-lips after nasal administration,[17] three normal mice were provided 10 μg/kg bFGF-lips solution 5 consecutive times, each at an interval of 30 min. The mice were killed 90 minutes after the last administration, and brain regions, including the olfactory region, pallium, hippocampus, striatum and cerebrum, were separated. The distribution of nasally administered bFGF-lips in different brain regions was evaluated using Western blot analysis to detect bFGF expression in each brain region. Normal mice that received equal doses of intranasally administered blank-lips solution were used as controls for baseline control.

Morris Water Maze Test

On the 7th day after the intervention, the mice were subjected to spatial learning and memory tests with the Morris water maze (MWM). The MWM test was conducted in a circular tank (140 cm in diameter, 50 cm high) filled with opaque, white water (22–25°C) in a dimly lit room. One of the quadrants was equipped with an escape platform submerged 1.5 cm below the white water surface. Before starting the acquisition training, the mice were individually handled for 1 min for 2 days to habituate the mice to handling. The mice were then trained for 5 consecutive days, with four trials per day per mouse. During the training sessions, the mice were required to find the submerged platform. The training was completed as soon as the animals were located on the platform or when 60 seconds had elapsed. If the mouse could not find the platform in a given trial, the mouse was guided to the platform. The latency and distance traveled to reach the platform in each trial were tracked and recorded. On day 6, the platform was removed from the pool, and a single probe test was performed to measure the integrity and strength of spatial memory 24 h after the last training trial of the acquisition phase. The quadrant where the platform was located during training was referred to as the target quadrant. The time and percentage of time spent in the target quadrant as well as the number of crossings over the platform were measured as the results of the probe trial.[34]

Novel Object Recognition Test

The novel object recognition (NOR) test is a relatively fast and efficient method for testing learning and memory in mice. The NOR test relies on rodents' natural proclivity to explore novel objects.[35] The NOR tests were conducted in the experimental apparatus, which consisted of a rectangular box and three objects (A, B and C). Object A was the same as object B, while object C was obviously different from objects A and B. Prior to testing, the mouse was handled for 2 days to habituate the mice to handling. On the first and second days, the mouse could explore the area for 10 min. On day 3 of

the test, the mouse was placed in an opaque box together with two objects (A and B) and was left to explore the objects for 5 min, after which the mouse was returned to its home cage. After 60 min, the mouse was returned to the test box, in which object B had been replaced with object C at the same location, and the mouse could explore the object for 5 min. Object interaction was defined as when a mouse's head was within 2 cm of the object and directed toward the object. After each trial, the objects and box were cleaned with ethanol. The recognition index was calculated by dividing the amount of time spent exploring the novel object by the total time spent exploring both objects in the test.

Histopathological Examination

After behavioral evaluation, five mice randomly selected from each group were sacrificed, and their brains were harvested immediately for histopathological examination. Mouse brains were immersed in 10% neutral buffered formalin, embedded in paraffin and cut into 4-μm-diameter slices. Coronal sections of the dorsal hippocampus were prepared. Hematoxylin and eosin (HE) staining and Nissl staining were performed according to the instructions of the kits. Histopathological changes in the hippocampi of the mice were observed using a light microscope (Olympus BX53, Japan), and the number of neuronal cells was counted at 400× magnification.

TUNEL Staining

Terminal deoxynucleotidyl transferase dUTP nick end labeling (TUNEL) staining was conducted with a TUNEL Apoptosis Assay Kit (Roche Applied Science, Penzberg, Germany) according to the manufacturer's instructions. In brief, the hippocampal tissue sections were dewaxed in xylene and rehydrated in graded alcohol. Then, the slices were treated with PBS for 5 min and digested with 20 μg/mL protease K at 37°C for 20 min. The slices were incubated with 50 μL of TUNEL detection liquid, 5 μL of TdT enzyme and 45 μL of fluorescent liquid at 37°C in the dark for 60 min. TUNEL-positive cells were observed under a fluorescence microscope (Olympus, Tokyo, Japan) and counted using ImageJ software to calculate the apoptotic index (AI, AI=number of apoptotic neurons/total number of neurons).

ELISA

The remaining five mice in each group were decapitated under deep anesthesia. The hippocampal tissues were removed from the brain tissues on ice. PBS was added at a ratio of 1 g:9 mL (weight/volume), and the tissues were homogenized by ultrasound at low temperature. The supernatant was collected and stored after centrifugation (12,000 rpm, 4°C, 15 min). The hippocampal levels of superoxide dismutase (SOD), glutathione peroxidase (GSH-Px), malondialdehyde (MDA) and bFGF were measured using mouse ELISA kits (Nanjing Jiancheng Bioengineering Institute, Nanjing, Jiangsu, China) according to the manufacturer's instructions. The mean value of duplicate samples was taken as the final concentration for each animal.

Western Blot Analysis

Brain tissues were added to RIPA lysis buffer (RIPA:PMSF =100:1) (Beyotime Biotechnology Co., Ltd., Shanghai, China) at a ratio of 20 g:200 mL (weight/volume) after removal from the mouse brain. The tissues were homogenized by ultrasonication at low temperature for 20 min. After centrifugation at 14,000 × g at 4°C for 5 min, the supernatants were collected to measure the concentrations of bFGF, apoptosis-related proteins and phosphatidylinositol-3-kinase (PI3K)/protein kinase B (AKT) signaling pathway-related proteins. The total protein concentration was determined using a bicinchoninic acid (BCA) protein assay kit (Beyotime Biotechnology Co., Ltd., Shanghai, China). The total protein (40 μg) from each sample was separated by sodium dodecyl sulfate–polyacrylamide gel electrophoresis (12% gel) and transferred onto a nitrocellulose membrane. The membranes were blocked for 1 h at 37°C with bovine serum albumin in 0.1% Tween 20 in Tris-buffered saline (TBST). After blocking, the membranes were incubated with primary antibodies against bFGF (1:1000, Abcam), AKT (1:1000, Santa Cruz), phosphorylated AKT (P-AKT, 1:1000, Santa Cruz), B-cell lymphoma 2-associated X protein (Bax, 1:1000, Santa Cruz), B-cell lymphoma 2 (Bcl-2, 1:1000, Santa Cruz), caspase-3 (1:1000, Santa Cruz), nuclear factor erythroid 2-related factor 2 (Nrf2, 1:1000, Santa Cruz), NAD(P)H quinone oxidoreductase 1 (NQO1, 1:1000, Santa Cruz), haem oxygenase-1 (HO-1, 1:1000, Santa Cruz) and glyceraldehyde-3-phosphate dehydrogenase (GAPDH, 1:5000, Santa Cruz) at 4°C overnight. After being washed three times with TBST (ten minutes each), the membranes were subsequently incubated with horseradish peroxidase (HRP)-conjugated

secondary antibodies (1:5000, Santa Cruz) for 1 h at room temperature. Immunodetection was performed with an electrochemiluminescence (ECL) solution followed by exposure to X-ray film. The optical density of the bands was analyzed by ImageJ software.

Cell Culture

With reference to the published literature,[36] the human neuroblastoma cell line SH-SY5Y was used in this study to determine the safety and neuroprotective effects of bFGF-lips in vitro. The SH-SY5Y neuronal cells were cultured in Dulbecco's modified Eagle medium (DMEM) supplemented with 10% fetal bovine serum at 37 °C in a humidified atmosphere containing 5% CO_2.

Cell Viability

Cell viability was determined using 3-(4,5-dimethylthiazol-2-yl)-2,5-diphenyltetrazolium bromide (MTT, Beyotime). SH-SY5Y cells were treated with bFGF (bFGF-lips or bFGF solution, bFGF concentration = 0.3 mg/mL), blank-lips solution or PBS for 24 h, after which MTT (5 mg/mL) was added. Dimethyl sulfoxide (DMSO) was then added after the medium was removed. The mixture was shaken in the dark for 10 min, after which the absorbance was measured at 490 nm using an ELISA reader to evaluate the safety of bFGF-lips in vitro.

Oxygen–Glucose Deprivation/Reoxygenation Test

An oxygen–glucose deprivation/reoxygenation (OGD/R) test was used to evaluate the neuroprotective effect of bFGF-lips. For the OGD/R procedure,[37,38] SH-SY5Y cells were cultured in glucose-free or serum-free DMEM in an incubator with an atmosphere of 5% CO_2, 95% N2 or <0.1% O2 at 37°C for 2 h to initiate OGD insult. Then, the ischemic-hypoxic cells were stochastically separated into four groups as follows: the PBS group, blank-lips group, bFGF solution group (30 pg/mL), and bFGF-lips group (30 pg/mL) were incubated in fresh MEN/F12 medium containing the corresponding drug therapy interventions at 37°C under CO_2 for 24 hours. SH-SY5Y cells not subjected to OGD insult served as controls. After the OGD/R test, the cell viability of each group was detected by a MTT reagent. Moreover, the ROS concentration in each group was detected by an ROS assay kit (Beyotime) after OGD/R. ROS detection was conducted according to previous methods[39] and according to the kit instructions.

Statistical Analysis

The data are expressed as the mean±standard deviation. For the MWM data (latency to escape), repeated-measures mixed analysis of variance (ANOVA) with Bonferroni's post hoc correction was used to assess group and training day differences. The NOR test results (exploratory time) were analyzed using repeated-measures two-way ANOVA followed by Bonferroni's post hoc correction. The other results were analyzed by one-way ANOVA. A value of $P<0.05$ was considered to indicate statistical significance.

Results

Characterization of bFGF-Lips

The lipid composition of = bFGF-lips and blank-lips featured a mass ratio of HSPC: cholesterol =9:1. The morphologies of bFGF-lips and blank-lips were investigated using TEM. TEM images (Figure 1A) indicated that blank-lips and bFGF-lips were spherical vesicles with particle aggregation. Moreover, there was no significant difference in the morphology of the nanoliposomes before or after bFGF was loaded. The size distributions of the bFGF-lips and blank-lips are highlighted in Figure 1B. Dynamic light scattering was used to determine the average particle sizes of bFGF-lips and blank-lips, which were 108.78±7.23 nm and 102.45±3.63 nm, respectively. The polydispersity index (PDI) represents the distribution of the particle size. The PDIs of bFGF-lips and blank-lips were 0.137±0.05 and 0.098±0.02, respectively, which indicated that bFGF-lips and blank-lips approached a monodisperse stable system. Moreover, zeta potential measurements showed that the zeta potentials of bFGF-lips and blank-lips were −36.124±3.124 mV and −41.365 ±5.112 mV, respectively. Furthermore, 88.34±1.89% of the bFGF-lips were encapsulated.

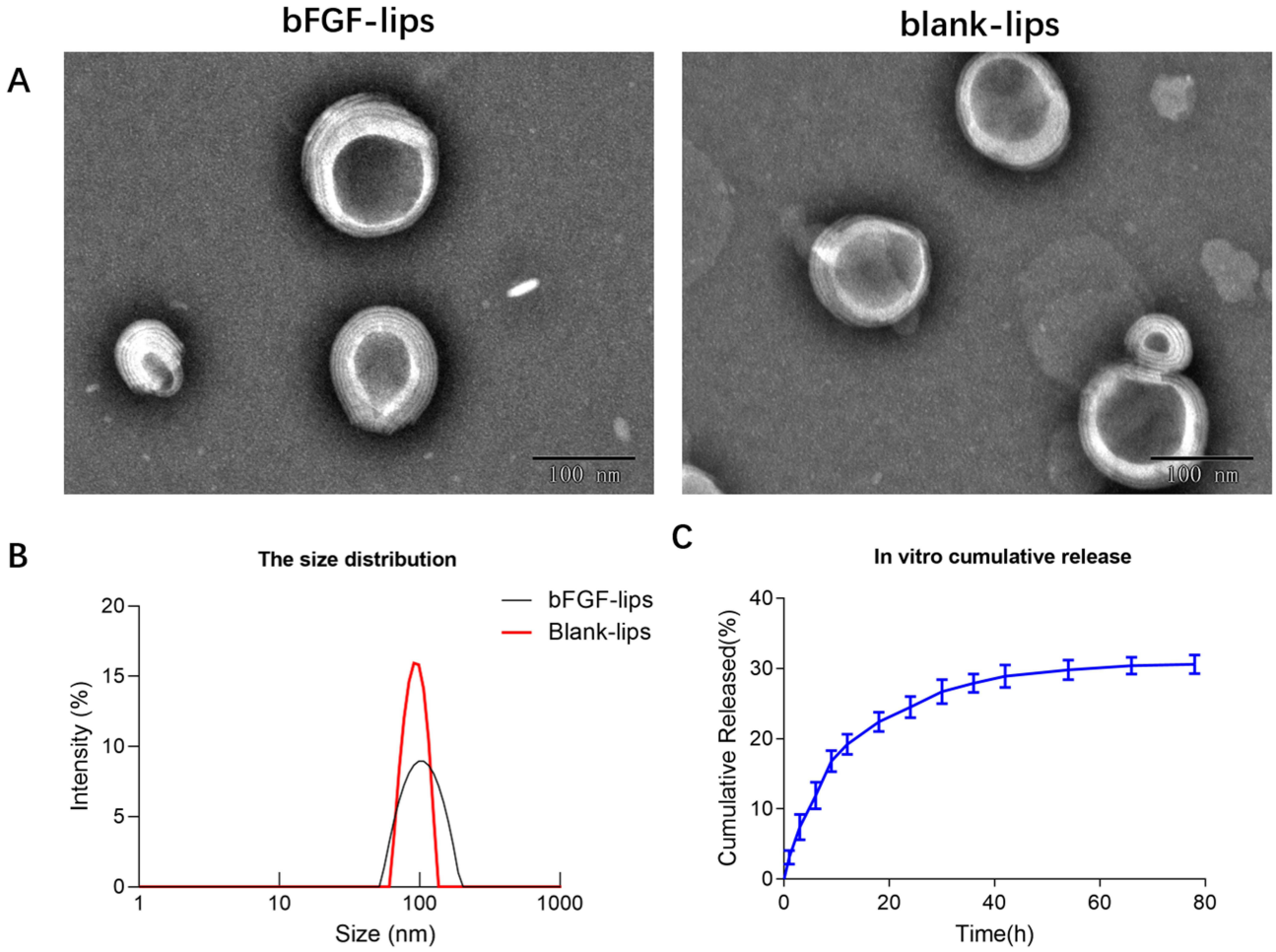

Figure 1 Characterization of the bFGF-lips and blank-lips. Transmission electron micrographs of bFGF-lips and blank-lips (**A**); the size distribution of bFGF-lips and blank-lips (**B**); in vitro cumulative release of bFGF-lips (**C**).

The in vitro drug release profiles of bFGF-lips in pH 7.4 PBS are shown in Figure 1C. The percentage of bFGF-lips released was only 19.20±1.64% at 12 h, 24.51±2.52% at 24 h and 30.63±1.33% at 78 h. The release of bFGF-lips was slow without obvious bursts. The stability test results showed that the K_E values at 4, 25, 30, 40 and 20±2°C at room temperature with light at 4100 lx for 10 days were 0.40, 1.82, 3.59, 14.47, and 3.10 times greater than those at 0 days, respectively (Table 1). The EE (%) was 12%, 24%, 30%, 42%, and 28% lower at these time points than on day 0 (Table 2). The bioactivity of bFGF-lips was 6%, 10%, 39%, 47%, and 26% lower than that on day 0 (Table 3). The results indicated that the three parameters were significantly influenced by temperature, especially high temperatures (30 and 40°C). Therefore, bFGF-lips solution should be stored at low temperature.

Table 1 Average of K_E Values (%) of bFGF-Lips on Various Condition ($\bar{x} \pm$ SD, n=3)

Condition	Time (Days)							
	0	1	3	5	10	30	60	90
4°C	1.26±0.02	1.48±0.08	1.51±0.11	1.63±0.11	1.77±0.19	2.73±0.55	3.81±0.74	4.02±0.34
25°C	1.26±0.11	1.51±0.14	1.65±0.28	1.75±0.14	3.55±0.31	4.01±0.47	4.23±0.35	4.81±0.19
30°C	1.26±0.06	2.01±0.18	3.34±0.27	4.93±0.44	5.78±0.77	9.67±1.11	23.71±3.13	35.74±2.71
40°C	1.26±0.05	2.33±0.27	4.53±0.39	7.37±0.32	19.49±2.71	21.8±3.43	32.57±3.72	49.45±4.03
Light (4100lx)	1.26±0.03	1.94±0.15	2.33±0.43	3.75±0.32	5.17±0.46			

Note: The experiments of highlight were studies for 10 days.

Table 2 Average of EE (%) of bFGF-Lips During Storage ($\bar{x} \pm SD$, n=3)

Condition	Time (Days)							
	0	1	3	5	10	30	60	90
4°C	89.12±2.13	84.32±4.77	79.53±3.14	78.32±5.71	78.47±3.77	75.29±7.13	71.34±6.59	70.49±5.91
25°C	89.12±3.75	82.38±6.14	76.39±4.77	70.48±6.39	68.15±4.01	58.12±5.34	50.48±5.71	42.37±6.39
30°C	89.12±3.37	78.49±7.31	74.93±5.83	67.14±4.39	62.12±6.14	50.34±3.17	39.14±4.01	27.46±5.47
40°C	89.12±3.21	73.29±5.77	70.72±4.74	64.39±5.03	51.58±4.83	31.71±4.44	21.31±7.49	11.12±3.63
Light (4100lx)	89.12±2.47	82.14±5.33	73.34±4.11	69.91±5.88	63.77±6.08			

Note: The experiments of highlight were studies for 10 days.

Table 3 Average of Bioactivity (×10^5IU/mL) of bFGF-Lips on Various Conditions ($\bar{x} \pm SD$, n=3)

Condition	Time (Days)							
	0	1	3	5	10	30	60	90
4°C	7.08±0.29	6.97±0.40	6.82±0.57	6.71±0.33	6.62±0.39	6.35±0.25	6.07±0.44	5.75±0.53
25°C	7.08±0.41	7.01±0.58	6.74±0.84	6.55±0.45	6.39±0.27	6.02±1.33	5.37±0.31	4.82±0.77
30°C	7.08±0.33	6.04±0.37	5.32±0.43	4.97±0.27	4.31±0.28	3.28±0.24	2.31±0.29	1.47±0.16
40°C	7.08±0.18	5.65±0.22	5.27±0.39	4.08±0.32	3.72±0.23	2.74±0.18	1.23±0.13	0.55±0.07
Light (4100lx)	7.08±0.27	6.52±0.34	6.17±0.71	5.57±0.39	5.24±0.47			

Note: The experiments of highlight were studies for 10 days.

Nasal Administration of bFGF-Lips Enhanced Exogenous bFGF Levels in Different Brain Regions

To evaluate the brain region distributions of bFGF-lips after nasal administration, Western blotting was performed and the bFGF levels were determined in the olfactory region, pallium, hippocampus, striatum and cerebrum 90 min post-IN. As shown in Figure 2A and B, compared with those in the control group, the levels of exogenous bFGF in each brain region were significantly increased by the intranasal administration of bFGF-lips. Moreover, the results showed the distribution of bFGF-lips in different brain regions after nasal administration. The distribution order of bFGF-lips from high to low was region, pallium, hippocampus, striatum and cerebrum.

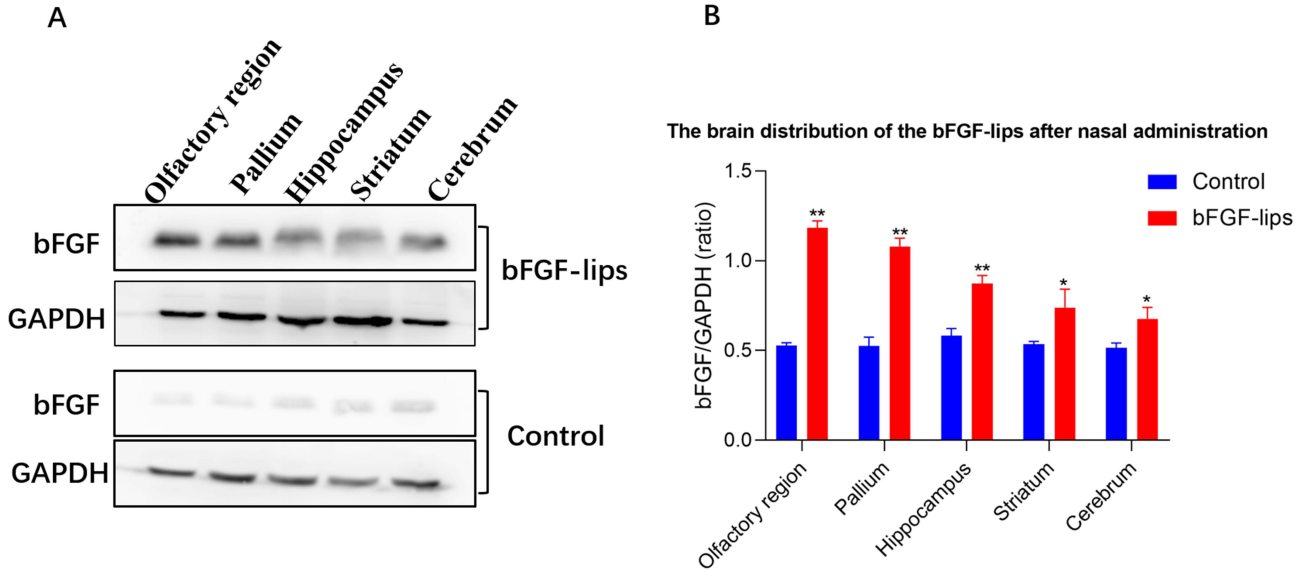

Figure 2 Nasal administration of bFGF-lips enhanced exogenous bFGF levels in different brain regions. (**A**) The expressions of bFGF in each brain region after nasal administration of bFGF-lips and blank-lips were analysed by Western blot. (**B**) The quantification data for Western blot analysis of bFGF. Data are presented as means±SDs (n=3). *P<0.05, **P<0.01 vs control group.

Nasal Administration of bFGF-Lips Improves the Learning and Memory Ability of VD Mice

The MWM and NOR tests were performed to investigate how the nasal administration of bFGF-lips affects the learning behavior of the experimental mice. In the MWM test, the average escape latencies of the mice were compared among the five days and among the five groups. As shown in Figure 3A and B, the VD mice exhibited a significantly longer escape latency than the sham mice on day 5 ($P<0.01$, increased by 0.45-fold). The latency to reach the platform was significantly shorter in the bFGF-lips group than in the bFGF group, blank-lips group and VD group on day 5 ($P<0.01$; reduced by 30%, 25% and 22%, respectively). No statistically significant differences were identified among the groups from training day 1 to day 4. In the probe test (Figure 3C and D), compared with sham group mice, VD group mice displayed significantly lower values for parameters assessing memory, ie, the time and the percentage of time spent in the target quadrant and the number of crossings over the platform area ($P<0.01$, respectively, decreased by 52%, 60% and 65%). Furthermore, the values attained for the memory parameters were significantly greater in the bFGF-lips group than in the

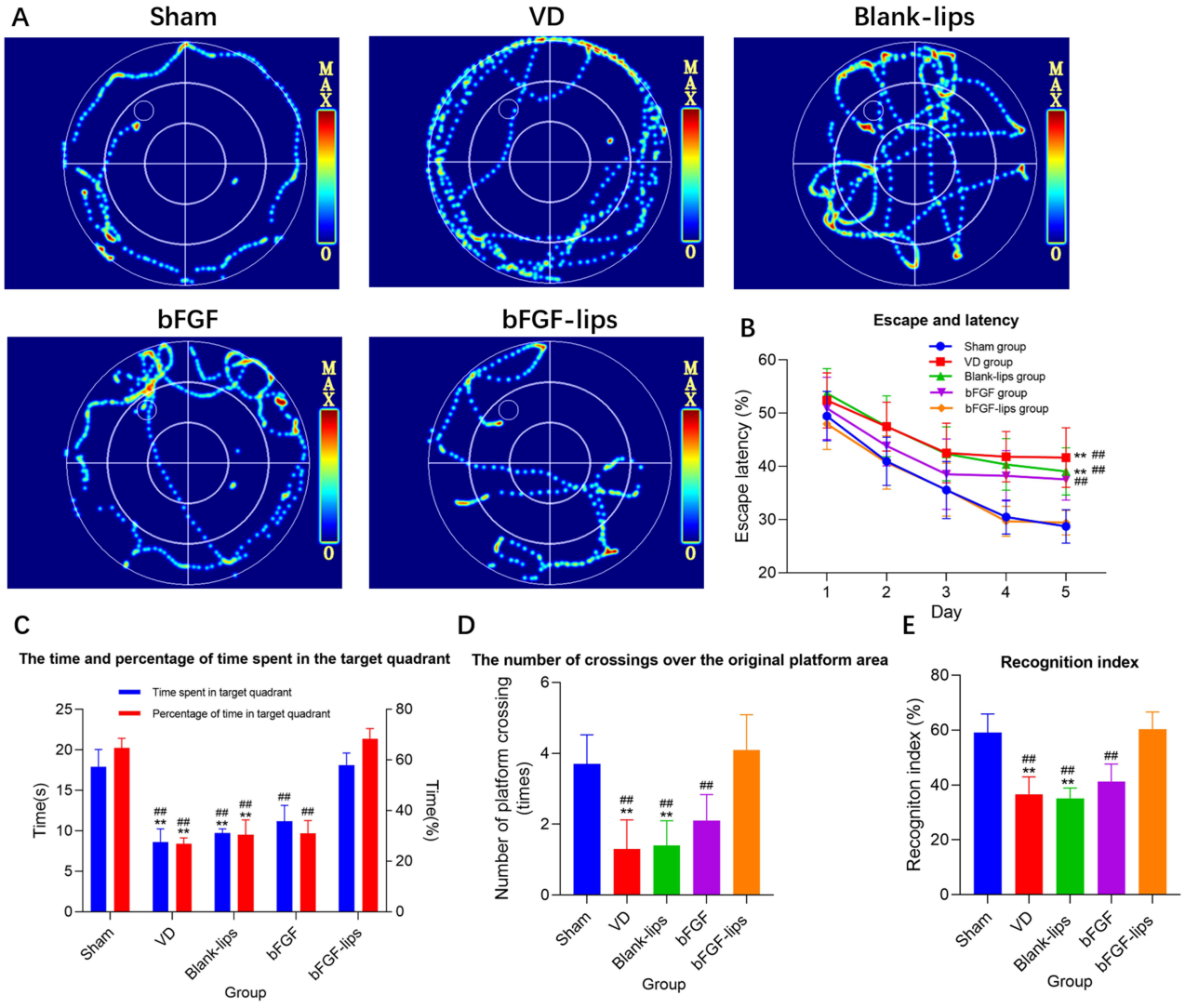

Figure 3 Nasal administration of bFGF-lips improved the learning and memory ability of VD mice. (**A**) Represents the video tracks of mice in each group on day 5 of the MWM test. (**B**) Represents escape and latency in the target quadrant. Two-way repeated-measures ANOVA with Bonferroni's post-hoc test was used for the statistical analysis of training data. The escape latency data were significantly different only on day 5. (**C**) Represents the time and percentage of time spent in the target quadrant. (**D**) Represents the number of crossings over the original platform area. (**E**) Represents the recognition index. Data other than the escape latency were analysed by one-way ANOVA. Data are presented as means±SDs (n=10). **P<0.01 vs sham group; ##P<0.01 vs bFGF-lips group.

VD group (increased by 1.11-, 1.55- and 2.15-fold, respectively), blank-lips group (increased by 0.86-, 1.24- and 1.9-fold, respectively) and bFGF group (increased by 0.62-, 1.21- and 0.95-fold, respectively) (P<0.01).

Moreover, we performed the NOR test to investigate the effects of bFGF-lips on the short-term memory of the experimental mice. The results (Figure 3E) showed that the recognition index of the VD group was significantly lower than that of the sham group (P<0.01, reduced by 38%). Among the intervention groups, the cognitive indices of the bFGF-lips group were significantly greater than those of the blank-lips group, bFGF group and VD group (increased by 0.71-, 0.46- and 0.64-fold, respectively), which were close to those of the sham group.

Nasal Administration of bFGF-Lips Alleviates Neuronal Injury and Loss in the Hippocampus of VD Mice

HE and Nissl staining were performed to assess the neuroprotective effects of intranasal administration of bFGF-lips on the hippocampal CA1 region of brain tissues. The results showed that the pyramidal neurons in the hippocampal CA1 region in sham group mice were aligned, with round nuclei, clear margins and nucleoli, transparent cytoplasm, and uniform distribution of chromatin in the nuclei. In contrast, pathological abnormalities, in which neurons were arranged in a scattered pattern, along with neuron shrinkage and loss were observed in the VD group (P<0.01; Figure 4A and B). The number of neurons in the VD group was 36% lower than that in the sham group. However, bFGF-lips treatment alleviated these histopathological alterations and reversed the hippocampal CA1 region neuron loss compared with the VD group and other intervention groups (P<0.01). The number of neurons in the bFGF-lips group was 0.52-, 0.54-, 0.41-fold higher than those in the VD group, blank-lips group and bFGF group, respectively.

As shown in Figure 4C and D, neurons of sham group mice exhibited a normal morphology with clear Nissl bodies in the cytoplasm, while the neurons of VD group mice showed a scattered arrangement, and the number of Nissl-positive cells was significantly decreased (P<0.01, decreased by 41%). After nasal administration of bFGF-lips, the morphology and arrangement of neurons in the CA1 region were obviously improved and the number of Nissl-positive cells was significantly increased compared with the VD group and other intervention groups (P<0.01). The number of neurons in the bFGF-lips group was 0.63-, 0.62-, and 0.52-fold higher than those in the VD group, blank-lips group and bFGF group, respectively.

Nasal Administration of bFGF-Lips Inhibits Neuronal Apoptosis in the Hippocampus of VD Mice

TUNEL staining was performed to determine the AI of neurons in the hippocampal CA1 region of mice. TUNEL staining (Figure 5A) results showed that TUNEL-positive granules exhibited green fluorescence. As shown in Figure 5B, significantly increased AI was observed in the hippocampal CA1 area neurons of VD group mice compared with sham group mice (P<0.01, increased by 2.2-fold). A significantly decreased AI in hippocampal CA1 area neurons was observed in the bFGF-lips group compared with the VD group, blank-lips group and bFGF group (P<0.01, decreased by 61%, 58% and 55%, respectively). No obvious difference in the AI of neurons in the hippocampal CA1 region was observed between the sham group and the bFGF-lips group (P>0.05).

Nasal Administration of bFGF-Lips Prevents VD-Induced Oxidative Stress in the Hippocampus

The levels of SOD, MDA, GSH-Px and bFGF were measured with ELISA kits to evaluate the degree of oxidative stress in the hippocampi of the mice.[40] As depicted in Figure 6A–D, VD group mice showed an increase in the hippocampal oxidative stress marker MDA (P<0.01, increased by 1.99-fold) and decreases in the hippocampal antioxidant markers SOD, GSH-Px and bFGF (P<0.01, decreased by 60%, 23% and 59%) compared with sham group mice. Among all interventions, only nasal administration of bFGF-lips prevented the VD-induced increase in the hippocampal MDA level (65%, 66% and 57% lower than those in the VD group, blank-lips group and bFGF group, respectively) as well as the decreases in the hippocampal antioxidant markers SOD (1.33-, 1.41- and 1.06-

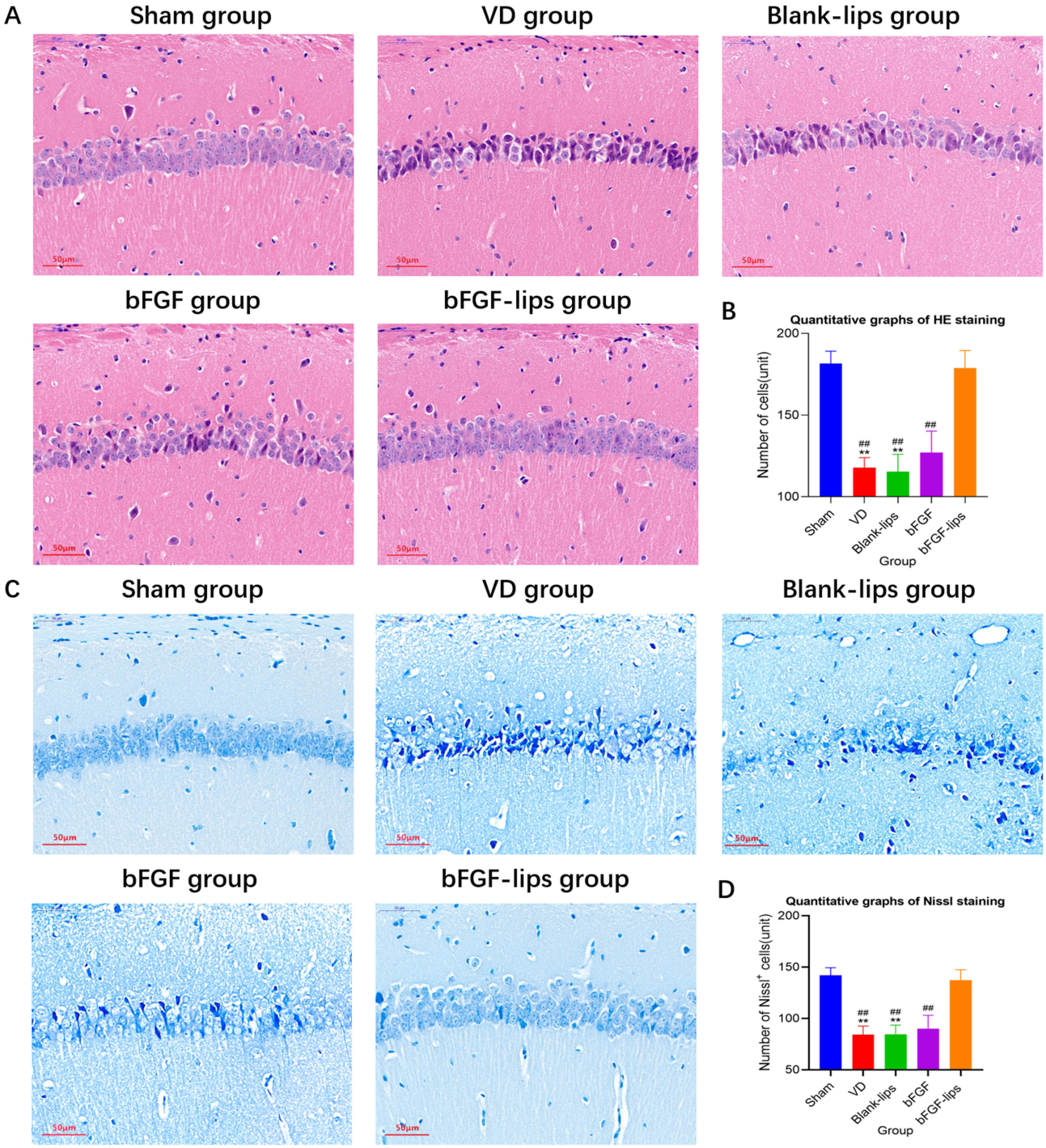

Figure 4 Nasal administration of bFGF-lips alleviated neuronal injury and loss in the hippocampi of VD mice. (**A**) Representative images of HE staining (400×). (**B**) Quantitative graphs of HE staining. (**C**) Representative images of Nissl staining (400×). (**D**) Quantitative graphs of Nissl staining. Data are presented as means±SDs (n=5). **P<0.01 vs sham group; ##P<0.01 vs bFGF-lips group.

fold higher than those in the VD group, blank-lips group and bFGF group, respectively), GSH-Px (P<0.01, 0.27-, 0.29- and 0.22-fold higher than those in the VD group, blank-lips group and bFGF group, respectively) and bFGF (2.88-, 3.00- and 0.74-fold higher than those in the VD group, blank-lips group and bFGF group, respectively) (P<0.01).

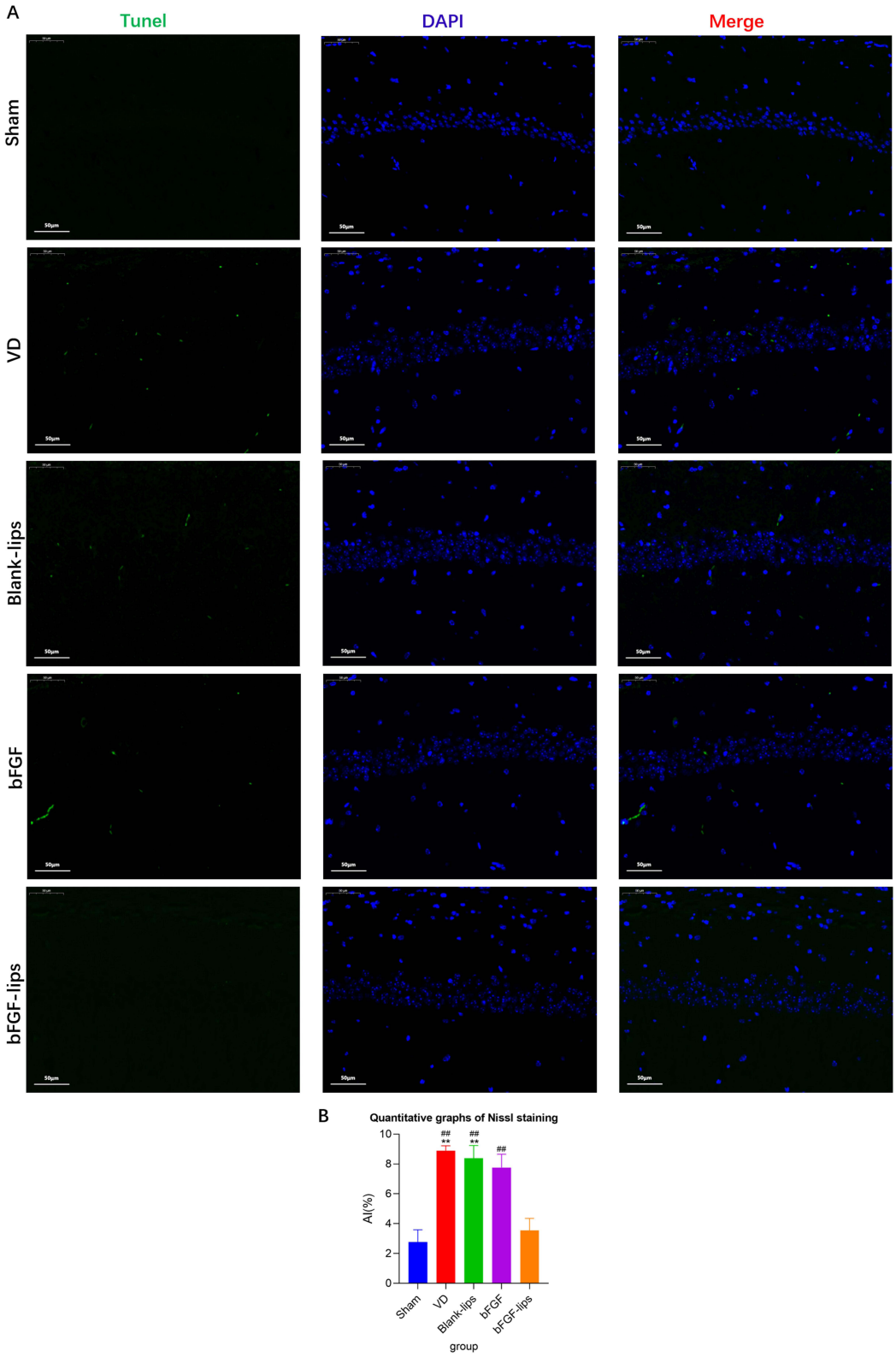

Figure 5 Nasal administration of bFGF-lips inhibited neuronal apoptosis in the hippocampi of VD mice. (**A**) Representative images of TUNEL staining (400×). (**B**) Quantitative graphs of TUNEL staining. Data are presented as means±SDs (n=5). **P<0.01 vs sham group; ##P<0.01 vs bFGF-lips group.

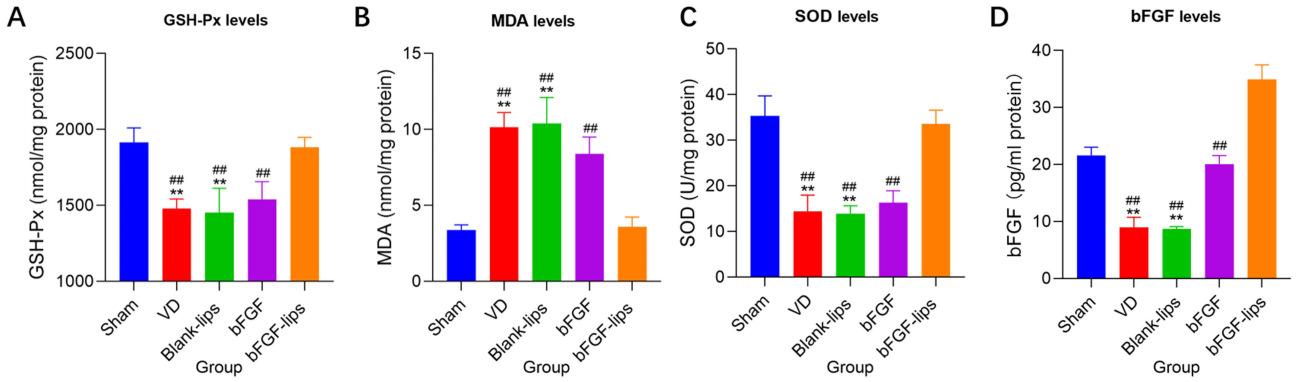

Figure 6 Nasal administration of bFGF-lips prevented VD-induced oxidative stress in the hippocampus. (**A**) GSH-Px levels. (**B**) MDA levels. (**C**) SOD levels. (**D**) bFGF levels. Data are presented as means±SDs (n=5). **P<0.01 vs sham group; ##P<0.01 vs bFGF-lips group.

Effects of Nasal bFGF-Lips Administration on the Concentrations of bFGF, Apoptosis-Related Proteins and PI3K/AKT-Signaling-Pathway-Related Proteins in Hippocampal Tissues

The concentration of bFGF in hippocampal tissues was measured by Western blot analysis to evaluate the efficiency of bFGF-lips delivery through nasal administration into the brain. As shown in Figure 7A and C, the concentrations of bFGF were significantly decreased in the VD group and blank-lips group compared with the sham group (P<0.05, declined by 66% and 61%). After different interventions, only nasal administration of bFGF-lips could significantly increase the concentration of bFGF in the hippocampal tissues compared with the concentrations observed in the VD group, blank-lips group and bFGF group (P<0.01, respectively increased by 3.85-, 3.22- and 0.68-fold).

To further elucidate the mechanism by which bFGF-lips reverses memory deficit in VD mice, we measured the concentrations of apoptosis-related proteins and PI3K/AKT-signaling-pathway-related proteins via Western blot analysis. As shown in Figure 7A, B and D–J, we found that the concentrations of the apoptosis-related proteins Bax (P<0.01) and caspase-3 (P<0.01) were significantly increased in the VD group (by 2.58- and 1.68-fold, respectively) and blank-lips group (by 2.94- and 1.69-fold, respectively) compared with the sham group, while the concentrations of the anti-apoptosis-related protein Bcl-2 (P<0.01) and the antioxidant-stress-related proteins PAKT (P<0.05), Nrf2 (P<0.01), NQO1 (P<0.05) and HO-1 (P<0.01) were significantly decreased in the VD group (by 60%, 45%, 42%, 38% and 76%, respectively) and blank-lips group (by 58%, 42%, 42%, 38% and 76%, respectively) compared with the sham group. Furthermore, the bFGF-lips group contained significantly increased concentrations of the anti-apoptosis-related protein Bcl-2 (P<0.01) and the antioxidant-stress-related proteins PAKT (P<0.01), Nrf2 (P<0.01), NQO1 (P<0.01) and HO-1 (P<0.01) compared with those in the VD group (increased by 3.53-, 1.62-, 1.28-, 1.06- and 5.17-fold, respectively) and bFGF group (increased by 1.56-, 0.59-, 0.67-, 0.94- and 1.3-fold, respectively). The concentrations of the apoptosis-related proteins Bax (P<0.01) and caspase-3 (P<0.01 vs VD group, P<0.05 vs bFGF group) in the bFGF-lips group were significantly lower than those in the VD group (56% and 52% lower, respectively) and the bFGF group (53% and 40% lower, respectively).

Evaluation of the Neuronal Toxicity and Neuroprotective Effect of bFGF-Lips Against OGD/R-Induced Injury in vitro

An MTT assay was performed with SH-SY5Y cells after they were treated with high concentration blank-lips, bFGF or bFGF-lips solutions to evaluated the cellular cytotoxicity in neuronal cells. The result showed that cell viability was not significantly different after treatment with high concentration of bFGF solution, bFGF-lips solution or blank-lips solution compared with PBS control group (Figure 8A).

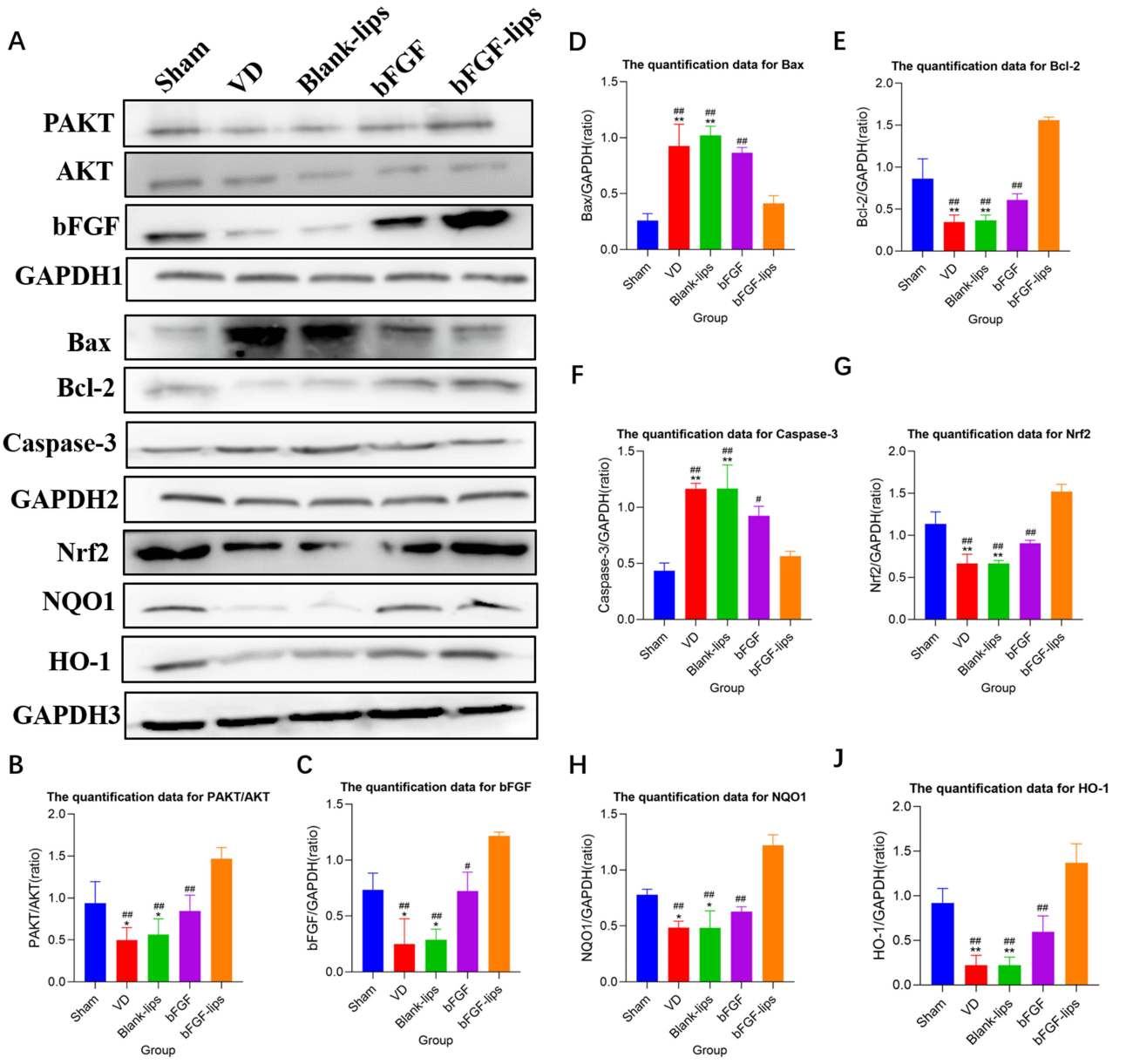

Figure 7 Effects of nasal administration bFGF-lips on the concentrations of bFGF, apoptosis-related proteins and PI3K/AKT-signalling-pathway-related proteins in hippocampal tissues. (**A**) Concentrations of bFGF, PAKT, AKT, Bcl-2, Bax, caspase-3, Nrf2, NQO1 and HO-1 in hippocampal tissues as detected by Western blot analysis. (**B–J**) The quantification data for Western blot analysis of PAKT/AKT, bFGF, Bax, Bcl-2, caspase-3, Nrf2, NQO1 and HO-1. Data are presented as means±SDs (n=5). *P<0.05, **P<0.01 vs sham group; #P<0.05, ##P <0.01 vs bFGF-lips group.

In the OGD/R test, the cells in the PBS group, blank-lips group and bFGF group showed significantly lower cell viabilities and higher ROS levels compared with those of the control group. Compared with PBS group, blank-lips group and bFGF group, the SH-SY5Y cells treated with low concentration bFGF-lips had higher cell viability and lower ROS level after OGD/R injury (Figure 8B and C).

Discussion

As a multifunctional cytokine, bFGF effectively protects neurons from a variety of insults, such as glutamate excitotoxicity, ischemia–reperfusion injury, hypoglycemia, intracellular calcium ion overload, and free radicals.[41] As a novel drug delivery system (DDS), nanoliposomes have potential as useful carriers for targeting the brain without toxicity in the nasal mucosa and CNS.[23] Moreover, using nanoliposomes to encapsulate proteins can not only prevent protein

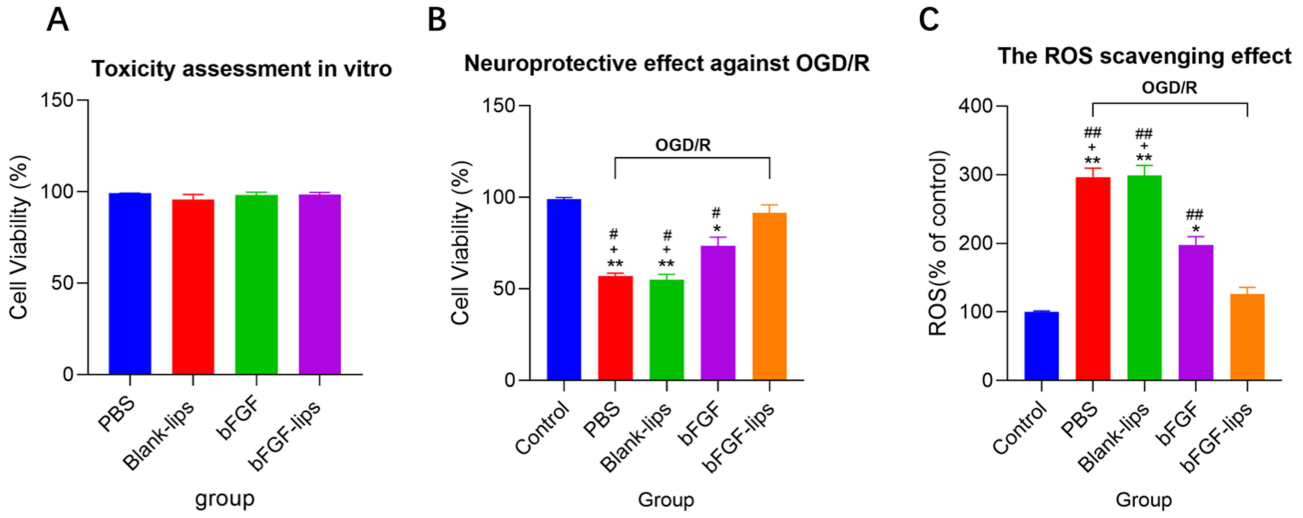

Figure 8 Evaluation of neuronal toxicity and neuroprotective effect of bFGF-lips against OGD/R induced injury in vitro. (**A**) The results of neuronal cell viabilities assessed by MTT after in vitro neuronal toxicity test. (**B**) The results of neuronal cell viabilities assessed by MTT after ODG/R test. (**C**) The result of ROS levels of neuronal cell after ODG/R test. Data are presented as means±SDs (n=3). *P<0.05, **P<0.01 vs control group; $^{+}$P<0.05, vs bFGF group; $^{\#}$P<0.05, $^{\#\#}$P <0.01 vs bFGF-lips group.

enzymatic degradation and increase protein uptake by cells but also increase protein residence time in the nasal cavity and promote protein transport across the nasal mucosa.[23]

In this study, we used the reverse-phase evaporation method to prepare bFGF-lips. Compared with the previously reported two-step preparation technology,[17] the method used to prepare bFGF liposomes in this study is simpler, quicker, more repeatable and suitable for promotion. The average particle size and zeta potential of bFGF-lips were 108.78±7.23 nm and −41.365±5.112 mV, respectively. The size and zeta potential of the nanoliposomes are key factors that affect nasal administration efficiency. Khan, Liu, Khan, Zhai[23] reported that nanoliposomes with particle sizes in the range of 100–200 nm could be transported from the nose to the brain through caveolae-mediated endocytosis. Nanoliposomes suitable for nasal delivery must have an absolute zeta potential >30 to prevent static repulsion on approach and facilitate nanoliposome-cell interaction.[23] Since the absolute value of Zeta of bFGF nanoliposomes prepared in our previous study[17] was only 15.3±1.6 mv, the bFGF-lips prepared in this study are more suitable for nasal administration according to the above requirements. The bFGF-lips encapsulation rate was 88.34±1.89%, which indicated that nanoliposomes were suitable for the encapsulation of bFGF. In vitro cell experiments showed that bFGF-lips or blank-lips did not affect the activity of nerve cells even in high concentrations, indicating that the bFGF-lips exhibited high biosafety. Western blot analysis and ELISA detection of the concentration of bFGF in hippocampal tissues showed that the bFGF concentration in the VD group was significantly lower than that in the sham group, which was consistent with the findings of a previous study.[42] However, the bFGF concentration in the bFGF-lips group was significantly higher than that in the bFGF group and other intervention groups. The result confirmed that using nanoliposomes to encapsulate bFGF combined with nasal administration could effectively deliver the protein to the brain and thus significantly increase the bFGF concentration in the brain for the treatment of VD.

Moreover, according to previous reports,[20] the liposomal lipid membrane that loads macromolecular drugs in the nose–brain pathway is composed mainly of different phospholipids and cholesterol. Drug-carrying nanoliposomes prepared by different phospholipids exhibit different potential and different efficiency of drug delivery from the nasal cavity to the brain. Under the same particle size conditions, PEGylated liposomes prepared by adding PEGylated phospholipids to the liposome phospholipid membrane may exhibit an increased efficiency of drug entry into the brain and an increased retention time in the brain. In addition, positively charged liposomes may result in increased retention time of drugs in the olfactory epithelial cells, thus improving the permeability of drug delivery in the nose–brain pathway. Although the liposomes prepared in this study did not contain PEG and were negatively charged, our findings confirm that bFGF-coated liposomes can significantly increase the content of bFGF in the brain after nasal administration.

Therefore, we will further optimize our lipid composition and preparation process in subsequent experimental studies to improve the efficiency of drug delivery in the brain.

In this animal study, we investigated the protective effects of bFGF-lips on VD mice. VD is a disease complicated by brain injury and manifests as severe cognitive impairment and memory loss.[43] The MWM and NOR tests are reliable paradigms used to assess spatial learning and memory in laboratory animals.[44,45] Recently, several studies have reported that repeated cerebral ischemia–reperfusion can cause learning and memory impairment and eventually lead to VD.[46,47] Consistent with these studies, our MWM and NOR test results showed that the learning and memory function of VD group mice, in which VD was induced by repeated cerebral ischemia–reperfusion, were obviously impaired. This impairment was characterized by a longer latency to find the submerged platform during the navigation trial, a longer escape latency, fewer crossings over the platform, and a lower percentage of time spent in the target quadrant during the probe trial in the MWM test as well as a lower recognition index in the NOR test. Moreover, the hippocampus plays a critical role in memory and spatial cognition.[48] Within the hippocampal memory system, CA1 neurons are critically involved the formation, consolidation, and retrieval of hippocampus-dependent memories.[49] Obvious histopathological changes were reported in the hippocampal CA1 region of mice that underwent repeated cerebral ischemia–reperfusion.[50] Consistent with this previous study, the results of histopathological examinations in this study, including HE, Nissl and TUNEL staining, showed that the hippocampal CA1 region of VD group mice also displayed significant histopathological lesions, such as a scattered arrangement of neurons and neuron shrinkage and loss. Furthermore, compared to mice in other groups, VD group mice showed fewer Nissl-positive cells and more apoptotic cells. The above results confirmed that a mouse model of VD was successfully established in this study. We found that nasal administration of bFGF-lips significantly ameliorated the cognitive impairments induced by repeated cerebral ischemia–reperfusion, as evidence by improvements in the behavioral abnormalities and histopathology lesions in bFGF-lips group mice compared with VD group mice. However, nasal administration of bFGF solution only partially restored memory deficits in VD mice. Taken together, our research results suggest that nasal administration of bFGF-lips can effectively increase the bFGF concentration in the hippocampus so that bFGF can attenuate memory deficits in VD model mice.

This study also investigated the mechanism by which bFGF-lips nasal administration reverses the memory deficits of VD mice. As previously reported, apoptosis, which refers to the process of programmed cell death, plays a major role in the development and pathogenesis of VD.[51,52] Various apoptotic proteins and regulatory pathways have been found to participate in the regulation of cell apoptosis progression. Bcl-2, Bax and caspase-3 participate in the apoptosis signal transduction mechanism and play irreplaceable roles in apoptosis. When Bcl-2 is upregulated, the Bcl-2/Bax heterodimer forms with bax protein. The Bcl-2/Bax heterodimer acts as a molecular switch on the mitochondrial permeability transition pore to regulate its opening degree, reduce ion channel activity, restrict some small molecules (such as CytC) from entering the cytoplasm, and finally inhibit apoptosis.[53] Previous study have found that upregulating the expression of Bcl-2 and reducing the expression of bax can significantly restrict the release of CytC, inhibit the activation of caspase-3 and the occurrence of apoptosis, and exert significant neuroprotective effects on VD rats.[52] Similar to these previous studies, in this study, the concentrations of Bax and caspase-3 were significantly increased and the concentration of Bcl-2 was reduced in VD group mice. However, nasal administration of bFGF-lips reduced the concentrations of Bcl-2, Bax, and caspase-3 and thereby reduced neuronal apoptosis. Therefore, regulating the levels of apoptosis-related factors to inhibit neuronal apoptosis is among the molecular mechanisms by which nasal administration of bFGF-lips attenuates repeated cerebral ischemia–reperfusion-induced cognitive impairments (Figure 9).

The overproduction of ROS due to ischemia is a critical contributor to the pathogenesis of VD.[54,55] Recent studies reported that cerebral ischemia–reperfusion increased the generation of free radicals, which had direct toxic effects on neurons and could induce the apoptosis of nerve cells.[53,56] MDA is an important indicator of lipid peroxidation. SOD and GSH are free radical scavengers that can protect brain tissues against oxidative damage.[57,58] The levels of MDA, SOD and GSH reflect the degree of oxidative stress.[59] Previous research found that the levels of MDA, GSH and SOD in brain tissue were abnormal after repeated cerebral ischemia–reperfusion,[46] and our data was consistent with these findings, as the levels of MDA, SOD and GSH in the hippocampi of VD group mice were abnormal after repeated cerebral ischemia–reperfusion. However, nasal administration of bFGF-lips could effectively attenuate the abnormal oxidative stress in VD mice by significantly decreasing the levels of MDA and increasing the levels of GSH and SOD. OGD/R is widely used to

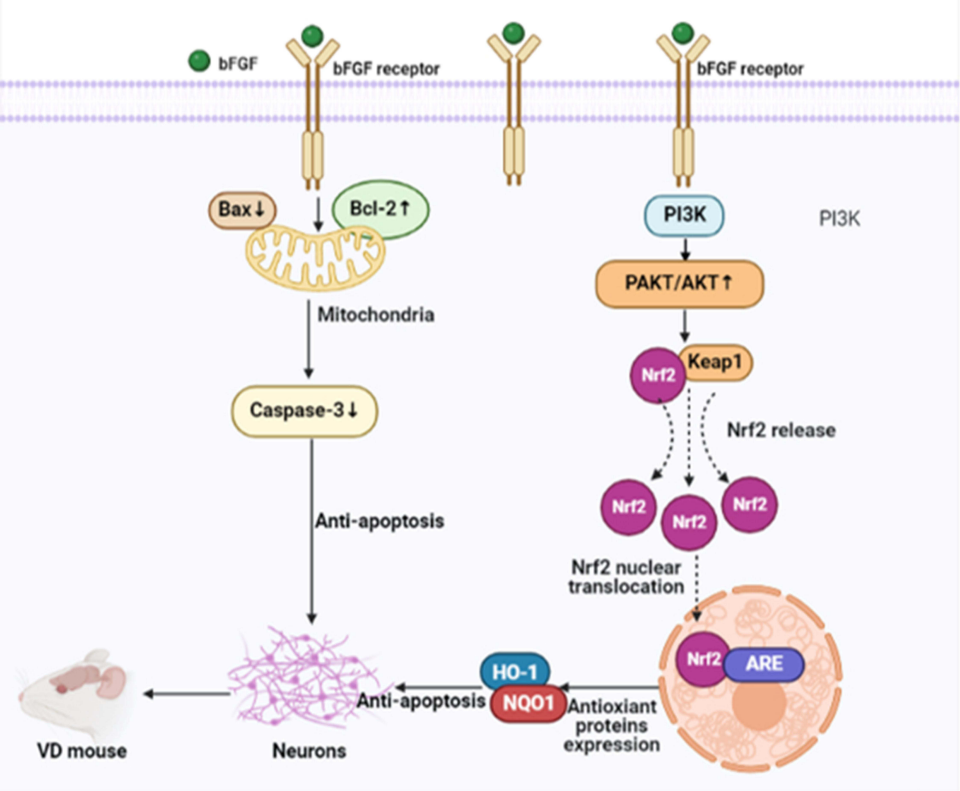

Figure 9 Molecular mechanisms of the bFGF reversal of neuronal apoptosis in VD mice through the regulation of the concentrations of apoptosis-related proteins and the activation of the PI3K/AKT/Nrf2 signalling pathway to inhibit oxidative stress.

study the neuronal cells model of brain ischemia–reperfusion injury in vitro.[36,60] Consistent with the results of animal experiments, OGD/r test confirmed that compared with PBS control group and bFGF group, bFGF-lips can significantly reduce the ROS level of nerve cells after ischemia–reperfusion, and the cell activity is effectively improved as a result.

The molecular mechanism underlying the effects caused by nasal administration of bFGF-lips on oxidative-stress-induced injury was preliminarily investigated in this study. A recent study showed that the activation of the phosphatidylinositol 3-kinase/protein kinase B (PI3K/AKT) signaling pathway plays a vital role in the protection of neurons against oxidative stress.[61] The activation of the PI3K/AKT signaling pathway leads to an increase in the PAKT/AKT ratio, the dissociation of nuclear factor erythroid 2-related factor 2 (Nrf2) from Kelch-like ECH-associated protein 1 (Keap1), and then the facilitation of Nrf2 nuclear translocation.[62] Intranuclear Nrf2 can then bind to the antioxidant response element (ARE), thereby initiating the transcription of numerous antioxidant enzymes, including HO-1 and NQO1,[63] that are involved in the detoxification of free radicals, thereby maintaining cellular redox homeostasis.[64] Previous studies, including ours, found that when bFGF is bound to its receptor, it could play an antioxidant role by activating the PI3K/AKT signaling pathway in a variety of experimental animal models, including models of myocardial infarction,[65] diabetic cardiomyopathy[30] and so on. According to our research, nasal administration of bFGF-lips could significantly increase the PAKT/AKT ratio and the concentrations of Nrf2, NQO1 and HO-1 compared with the observations in VD. These results indicated that bFGF-lips may inhibit oxidative stress by activating the PI3K/AKT/Nrf2 signaling pathway, thereby reducing neuronal apoptosis. The inhibition of oxidative stress through the activation of the PI3K/AKT/Nrf2 signaling pathway may be another molecular mechanisms by which nasal administration of bFGF-lips attenuates repeated cerebral ischemia–reperfusion-induced cognitive impairments (Figure 8).

Conclusion

In our study, we demonstrated that nasal administration of bFGF-lips significantly increased the bFGF concentrations in the hippocampi of VD mice. The bFGF then reduced the neuronal apoptosis induced by repeated ischemia–reperfusion

by regulating the expression of apoptosis-related proteins and activating the PI3K/AKT/Nrf2 signaling pathway to inhibit oxidative stress, ultimately improving cognitive impairment in VD mice.

Data Sharing Statement

The data that support the findings of this study are available from the first author, Ming Zhang, upon reasonable request.

Funding

This research was supported by Zhejiang Provincial Medical And Health Science And Technology Project (Grant No. 2021KY1068, 2021KY1067), Ningbo Natural Science Foundation (Grant No. 202003N4337, 202003N4295), Yinzhou District Science And Technology Project (Grant No. 2019AS0021, Grant No. Yinke 202045).

Disclosure

The authors report no conflicts of interest in this work.

References

1. Sharma B, Singh N. Pitavastatin and 4'-hydroxy-3'-methoxyacetophenone (HMAP) reduce cognitive dysfunction in vascular dementia during experimental diabetes. *Curr Neurovasc Res*. 2010;7(3):180–191. doi:10.2174/156720210792231831
2. Sharma B, Singh N. Attenuation of vascular dementia by sodium butyrate in streptozotocin diabetic rats. *Psychopharmacology*. 2011;215(4):677–687. doi:10.1007/s00213-011-2164-0
3. Gorelick PB, Scuteri A, Black SE, et al. Vascular contributions to cognitive impairment and dementia: a statement for healthcare professionals from the American heart association/American stroke association. *Stroke*. 2011;42(9):2672–2713. doi:10.1161/STR.0b013e3182299496
4. O'Brien JT, Thomas A. Vascular dementia. *Lancet*. 2015;386(10004):1698–1706. doi:10.1016/S0140-6736(15)00463-8
5. Toyama K, Koibuchi N, Uekawa K, et al. Apoptosis signal-regulating kinase 1 is a novel target molecule for cognitive impairment induced by chronic cerebral hypoperfusion. *Arterioscler Thromb Vasc Biol*. 2014;34(3):616–625. doi:10.1161/ATVBAHA.113.302440
6. Wang J, Jin H, Hua Y, Keep RF, Xi G. Role of protease-activated receptor-1 in brain injury after experimental global cerebral ischemia. *Stroke*. 2012;43(9):2476–2482. doi:10.1161/STROKEAHA.112.661819
7. Khan S, Yuldasheva NY, Batten TFC, Pickles AR, Kellett KAB, Saha S. Tau pathology and neurochemical changes associated with memory dysfunction in an optimised murine model of global cerebral ischaemia - a potential model for vascular dementia? *Neurochem Int*. 2018;118:134–144. doi:10.1016/j.neuint.2018.04.004
8. Siracusa R, Impellizzeri D, Cordaro M, et al. anti-inflammatory and neuroprotective effects of co-UltraPEALut in a mouse model of vascular dementia. *Front Neurol*. 2017;8:233. doi:10.3389/fneur.2017.00233
9. Lénárt N, Brough D, Dénes Á. Inflammasomes link vascular disease with neuroinflammation and brain disorders. *J Cereb Blood Flow Metab*. 2016;36(10):1668–1685. doi:10.1177/0271678X16662043
10. Zhu T, Zhu M, Qiu Y, et al. Puerarin alleviates vascular cognitive impairment in vascular dementia rats. *Front Behav Neurosci*. 2021;15:717008. doi:10.3389/fnbeh.2021.717008
11. Du SQ, Wang XR, Xiao LY, et al. Molecular mechanisms of vascular dementia: what can be learned from animal models of chronic cerebral hypoperfusion? *Mol Neurobiol*. 2017;54(5):3670–3682. doi:10.1007/s12035-016-9915-1
12. Cervellati C, Romani A, Seripa D, et al. Oxidative balance, homocysteine, and uric acid levels in older patients with Late Onset Alzheimer's Disease or Vascular Dementia. *J Neurol Sci*. 2014;337(1–2):156–161. doi:10.1016/j.jns.2013.11.041
13. Werner S, Unsicker K, von Bohlen Und Halbach O. Fibroblast growth factor-2 deficiency causes defects in adult hippocampal neurogenesis, which are not rescued by exogenous fibroblast growth factor-2. *J Neurosci Res*. 2011;89(10):1605–1617. doi:10.1002/jnr.22680
14. Woodbury ME, Ikezu T. Fibroblast growth factor-2 signaling in neurogenesis and neurodegeneration. *J Neuroimmune Pharmacol*. 2014;9(2):92–101. doi:10.1007/s11481-013-9501-5
15. Tang MM, Lin WJ, Zhang JT, Zhao YW, Li YC. Exogenous FGF2 reverses depressive-like behaviors and restores the suppressed FGF2-ERK1/2 signaling and the impaired hippocampal neurogenesis induced by neuroinflammation. *Brain Behav Immun*. 2017;66:322–331. doi:10.1016/j.bbi.2017.05.013
16. Guo ZH, Mattson MP. Neurotrophic factors protect cortical synaptic terminals against amyloid and oxidative stress-induced impairment of glucose transport, glutamate transport and mitochondrial function. *Cereb Cortex*. 2000;10(1):50–57. doi:10.1093/cercor/10.1.50
17. Zhao YZ, Lin M, Lin Q, et al. Intranasal delivery of bFGF with nanoliposomes enhances in vivo neuroprotection and neural injury recovery in a rodent stroke model. *J Control Release*. 2016;224:165–175. doi:10.1016/j.jconrel.2016.01.017
18. Lochhead JJ, Thorne RG. Intranasal delivery of biologics to the central nervous system. *Adv Drug Delivery Rev*. 2012;64(7):614–628. doi:10.1016/j.addr.2011.11.002
19. Mainardes RM, Urban MC, Cinto PO, Chaud MV, Evangelista RC, Gremião MP. Liposomes and micro/nanoparticles as colloidal carriers for nasal drug delivery. *Curr Drug Delivery*. 2006;3(3):275–285. doi:10.2174/156720106777731019
20. Hong SS, Oh KT, Choi HG, Lim SJ. Liposomal formulations for nose-to-brain delivery: recent advances and future perspectives. *Pharmaceutics*. 2019;11(10):540. doi:10.3390/pharmaceutics11100540
21. Fan Y, Chen M, Zhang J, Maincent P, Xia X, Wu W. Updated progress of nanocarrier-based intranasal drug delivery systems for treatment of brain diseases. *Crit Rev Ther Drug Carrier Syst*. 2018;35(5):433–467. doi:10.1615/CritRevTherDrugCarrierSyst.2018024697
22. Zhang C, Chen J, Feng C, et al. Intranasal nanoparticles of basic fibroblast growth factor for brain delivery to treat Alzheimer's disease. *Int J Pharm*. 2014;461(1–2):192–202. doi:10.1016/j.ijpharm.2013.11.049

23. Khan AR, Liu M, Khan MW, Zhai G. Progress in brain targeting drug delivery system by nasal route. *J Control Release*. 2017;268:364–389. doi:10.1016/j.jconrel.2017.09.001
24. Upadhyay P, Trivedi J, Pundarikakshudu K, Sheth N. Direct and enhanced delivery of nanoliposomes of anti schizophrenic agent to the brain through nasal route. *Saudi Pharm J*. 2017;25(3):346–358. doi:10.1016/j.jsps.2016.07.003
25. Tafaghodi M, Abolghasem Sajadi Tabassi S, Jaafari MR, Zakavi SR, Momen-Nejad M. Evaluation of the clearance characteristics of various microspheres in the human nose by gamma-scintigraphy. *Int J Pharm*. 2004;280(1–2):125–135. doi:10.1016/j.ijpharm.2004.05.009
26. Yuba E, Harada A, Sakanishi Y, Watarai S, Kono K. A liposome-based antigen delivery system using pH-sensitive fusogenic polymers for cancer immunotherapy. *Biomaterials*. 2013;34(12):3042–3052. doi:10.1016/j.biomaterials.2012.12.031
27. Aisha AF, Majid AM, Ismail Z. Preparation and characterization of nano liposomes of Orthosiphon stamineus ethanolic extract in soybean phospholipids. *BMC Biotech*. 2014;14:23. doi:10.1186/1472-6750-14-23
28. Dinda SC, Pattnaik G. Nanobiotechnology-based drug delivery in brain targeting. *Current Pharm Biotechnol*. 2013;14(15):1264–1274. doi:10.2174/13892010156661406081437 19
29. Sheng WS, Xu HL, Zheng L, et al. Intrarenal delivery of bFGF-loaded liposome under guiding of ultrasound-targeted microbubble destruction prevent diabetic nephropathy through inhibition of inflammation. *Artif Cells Nanomed Biotechnol*. 2018;46(sup2):373–385. doi:10.1080/21691401.2018.1457538
30. Zhao YZ, Zhang M, Tian XQ, Zheng L, Lu CT. Using basic fibroblast growth factor nanoliposome combined with ultrasound-introduced technology to early intervene the diabetic cardiomyopathy. *Int j Nanomed*. 2016;11:675–686. doi:10.2147/IJN.S99376
31. Xiang Q, Xiao J, Zhang H, et al. Preparation and characterisation of bFGF-encapsulated liposomes and evaluation of wound-healing activities in the rat. *Burns*. 2011;37(5):886–895. doi:10.1016/j.burns.2011.01.018
32. Zhang M, Yu WZ, Shen XT, et al. Advanced interfere treatment of diabetic cardiomyopathy rats by aFGF-loaded heparin-modified microbubbles and UTMD technique. *Cardiovasc Drugs Ther*. 2016;30(3):247–261. doi:10.1007/s10557-016-6639-4
33. He JT, Li H, Yang L, Cheng KL. Involvement of endothelin-1, H(2)S and Nrf2 in beneficial effects of remote ischemic preconditioning in global cerebral ischemia-induced vascular dementia in mice. *Cell Mol Neurobiol*. 2019;39(5):671–686. doi:10.1007/s10571-019-00670-y
34. Liu B, Kou J, Li F, et al. Lemon essential oil ameliorates age-associated cognitive dysfunction via modulating hippocampal synaptic density and inhibiting acetylcholinesterase. *Aging*. 2020;12(9):8622–8639. doi:10.18632/aging.103179
35. Lueptow LM. Novel object recognition test for the investigation of learning and memory in mice. *J Visualized Exp*. 2017;126:55718. doi:10.3791/55718
36. Fang YC, Chan L, Liou JP, et al. HDAC inhibitor protects chronic cerebral hypoperfusion and oxygen-glucose deprivation injuries via H3K14 and H4K5 acetylation-mediated BDNF expression. *J Cell Mol Med*. 2020;24(12):6966–6977. doi:10.1111/jcmm.15358
37. Zhuge XZ, Hu WX, Liu YM, et al. PD98059 protects SH-SY5Y cells against oxidative stress in oxygen-glucose deprivation/reperfusion. *Transl Neurosci*. 2023;14(1):20220300.
38. Yuan ZL, Mo YZ, Li DL, Xie L, Chen MH. Inhibition of ERK downregulates autophagy via mitigating mitochondrial fragmentation to protect SH-SY5Y cells from OGD/R injury. *Cell Commun Signaling*. 2023;21(1):204. doi:10.1186/s12964-023-01211-3
39. Xu J, Liu J, Li Q, et al. Pterostilbene alleviates Aβ(1-42) -induced cognitive dysfunction via inhibition of oxidative stress by activating Nrf2 signaling pathway. *Mol Nutr Food Res*. 2021;65(2):e2000711. doi:10.1002/mnfr.202000711
40. Yadav A, Sunkaria A, Singhal N, Sandhir R. Resveratrol loaded solid lipid nanoparticles attenuate mitochondrial oxidative stress in vascular dementia by activating Nrf2/HO-1 pathway. *Neurochem Int*. 2018;112:239–254. doi:10.1016/j.neuint.2017.08.001
41. Liu Y, Lu JB, Ye ZR. Permeability of injured blood brain barrier for exogenous bFGF and protection mechanism of bFGF in rat brain ischemia. *Neuropathology*. 2006;26(3):257–266. doi:10.1111/j.1440-1789.2006.00693.x
42. Wakayama K, Shimamura M, Yoshida S, et al. Prevention of vascular dementia via immunotherapeutic blockade of renin-angiotensin system in a rat model. *Brain Res*. 2021;1772:147667. doi:10.1016/j.brainres.2021.147667
43. Chen C, Chen W, Nong Z, et al. Hyperbaric oxygen alleviated cognitive impairments in mice induced by repeated cerebral ischemia-reperfusion injury via inhibition of autophagy. *Life Sci*. 2020;241:117170. doi:10.1016/j.lfs.2019.117170
44. Higaki A, Mogi M, Iwanami J, et al. Predicting outcome of Morris water maze test in vascular dementia mouse model with deep learning. *PLoS One*. 2018;13(2):e0191708. doi:10.1371/journal.pone.0191708
45. Sun M, Wu L, Chen G, Mo X, Shi C. Hemodynamic changes and neuronal damage detected by 9.4 T MRI in rats with chronic cerebral ischemia and cognitive impairment. *Brain Behav*. 2022;12(7):e2642. doi:10.1002/brb3.2642
46. Xue Y, Qu Z, Fu J, et al. The protective effect of astaxanthin on learning and memory deficits and oxidative stress in a mouse model of repeated cerebral ischemia/reperfusion. *Brain Res Bull*. 2017;131:221–228. doi:10.1016/j.brainresbull.2017.04.019
47. Xu J, Huai Y, Meng N, et al. L-3-n-butylphthalide activates Akt/mTOR signaling, inhibits neuronal apoptosis and autophagy and improves cognitive impairment in mice with repeated cerebral ischemia-reperfusion injury. *Neurochem Res*. 2017;42(10):2968–2981. doi:10.1007/s11064-017-2328-3
48. Moscovitch M, Cabeza R, Winocur G, Nadel L. Episodic memory and beyond: the hippocampus and neocortex in transformation. *Ann Rev Psychol*. 2016;67:105–134. doi:10.1146/annurev-psych-113011-143733
49. Bartsch T, Döhring J, Rohr A, Jansen O, Deuschl G. CA1 neurons in the human hippocampus are critical for autobiographical memory, mental time travel, and autonoetic consciousness. *Proc Natl Acad Sci USA*. 2011;108(42):17562–17567. doi:10.1073/pnas.1110266108
50. Gao L, Guo X, Liu S, et al. DL-3-n-butylphthalide imparts neuroprotection via Nrf2/SIRT3 pathway in a mouse model of vascular dementia. *Brain Res*. 2022;1779:147785. doi:10.1016/j.brainres.2022.147785
51. Li XJ, Hou JC, Sun P, et al. Neuroprotective effects of tongluojiunao in neurons exposed to oxygen and glucose deprivation. *J Ethnopharmacol*. 2012;141(3):927–933. doi:10.1016/j.jep.2012.03.042
52. Zhao T, Fu Y, Sun H, Liu X. Ligustrazine suppresses neuron apoptosis via the Bax/Bcl-2 and caspase-3 pathway in PC12 cells and in rats with vascular dementia. *IUBMB Life*. 2018;70(1):60–70. doi:10.1002/iub.1704
53. Annunziato L, Amoroso S, Pannaccione A, et al. Apoptosis induced in neuronal cells by oxidative stress: role played by caspases and intracellular calcium ions. *Toxicol Lett*. 2003;139(2–3):125–133. doi:10.1016/s0378-4274(02)00427-7
54. Choi DH, Lee KH, Kim JH, et al. NADPH oxidase 1, a novel molecular source of ROS in hippocampal neuronal death in vascular dementia. *Antioxid Redox Signaling*. 2014;21(4):533–550. doi:10.1089/ars.2012.5129

55. Guo S, Xu JJ, Wei N, et al. Honokiol attenuates the memory impairments, oxidative stress, neuroinflammation, and GSK-3β activation in vascular dementia rats. *J Alzheimers Dis*. 2019;71(1):97–108. doi:10.3233/JAD-190324
56. Manzanero S, Santro T, Arumugam TV. Neuronal oxidative stress in acute ischemic stroke: sources and contribution to cell injury. *Neurochem Int*. 2013;62(5):712–718. doi:10.1016/j.neuint.2012.11.009
57. Zarezadeh M, Baluchnejadmojarad T, Kiasalari Z, Afshin-Majd S, Roghani M. Garlic active constituent s-allyl cysteine protects against lipopolysaccharide-induced cognitive deficits in the rat: possible involved mechanisms. *Eur J Pharmacol*. 2017;795:13–21. doi:10.1016/j.ejphar.2016.11.051
58. Chen H, Yoshioka H, Kim GS, et al. Oxidative stress in ischemic brain damage: mechanisms of cell death and potential molecular targets for neuroprotection. *Antioxid Redox Signaling*. 2011;14(8):1505–1517. doi:10.1089/ars.2010.3576
59. Malinska D, Kulawiak B, Kudin AP, et al. Complex III-dependent superoxide production of brain mitochondria contributes to seizure-related ROS formation. *BBA*. 2010;1797(6–7):1163–1170. doi:10.1016/j.bbabio.2010.03.001
60. Wang D, Wang Y, Shan M, et al. Apelin receptor homodimer inhibits apoptosis in vascular dementia. *Exp Cell Res*. 2021;407(1):112739. doi:10.1016/j.yexcr.2021.112739
61. Ali T, Kim T, Rehman SU, et al. Natural dietary supplementation of anthocyanins via PI3K/Akt/Nrf2/HO-1 pathways mitigate oxidative stress, neurodegeneration, and memory impairment in a mouse model of Alzheimer's disease. *Mol Neurobiol*. 2018;55(7):6076–6093. doi:10.1007/s12035-017-0798-6
62. Thangapandiyan S, Ramesh M, Miltonprabu S, Hema T, Jothi GB, Nandhini V. Sulforaphane potentially attenuates arsenic-induced nephrotoxicity via the PI3K/Akt/Nrf2 pathway in albino Wistar rats. *Environ Sci Pollut Res Int*. 2019;26(12):12247–12263. doi:10.1007/s11356-019-04502-w
63. de Vries HE, Witte M, Hondius D, et al. Nrf2-induced antioxidant protection: a promising target to counteract ROS-mediated damage in neurodegenerative disease? *Free Radic Biol Med*. 2008;45(10):1375–1383. doi:10.1016/j.freeradbiomed.2008.09.001
64. Hayes JD, Dinkova-Kostova AT. The Nrf2 regulatory network provides an interface between redox and intermediary metabolism. *Trends Biochem Sci*. 2014;39(4):199–218. doi:10.1016/j.tibs.2014.02.002
65. Tong G, Liang Y, Xue M, et al. The protective role of bFGF in myocardial infarction and hypoxia cardiomyocytes by reducing oxidative stress via Nrf2. *Biochem Biophys Res Commun*. 2020;527(1):15–21. doi:10.1016/j.bbrc.2020.04.053